A design of Convolutional Neural Network model for the Diagnosis of the COVID-19

Xinyuan Song[1,a*]
[1]*Department of statistics and data science, National University of Singapore, Lower Kent Ridge Road 119077, Singapore*
[a]*Email: songxinyuan@pku.org.cn*
[*]*Corresponding Author*

Abstract

With the spread of COVID-19 around the globe over the past year, the usage of artificial intelligence (AI) algorithms and image processing methods to analyze the X-ray images of patients' chest with COVID-19 has become essential. The COVID-19 virus recognition in the lung area of a patient is one of the basic and essential needs of clicical centers and hospitals. Most research in this field has been devoted to papers on the basis of deep learning methods utilizing CNNs (Convolutional Neural Network), which mainly deal with the screening of sick and healthy people.In this study, a new structure of a 19-layer CNN has been recommended for accurately recognition of the COVID-19 from the X-ray pictures of chest. The offered CNN is developed to serve as a precise diagnosis system for a three class (viral pneumonia, Normal, COVID) and a four classclassification (Lung opacity, Normal, COVID-19, and pneumonia). A comparison is conducted among the outcomes of the offered procedure and some popular pretrained networks, including Inception, Alexnet, ResNet50, Squeezenet, and VGG19 and based on Specificity, Accuracy, Precision, Sensitivity, Confusion Matrix, and F1-score. The experimental results of the offered CNN method specify its dominance over the existing published procedures. This method can be a useful tool for clinicians in deciding properly about COVID-19.

Keywords: CNN (Convolutional Neural Network); COVID-19; early diagnosis; X-rays pictures of chest; Radiology images.

1. Introduction

Coronaviruses are a big classification of viruses ranging from the vius of common cold to the SARS causative agent. The initial version of Coronaviruse was revealed in 1965 and kept studying continuously till the mid-1980s. The structure of coronaviruses also has a typical RNA genome. The earlier work confirms that the people with co-morbidities and children with heart disease are at higher risk for coronaviruses[1]. Usually, the common cold is caused by the coronavirus. Coronaviruses, which are the second most common cause of colds after rhinoviruses, are more common in winter and spring.Most people become infected with coronavirus infections at some point in their lives, and most of these infections are not dangerous.

The current version of coronavirus; which causes Covid disease (SARS-CoV-2), is a significant exception in this family and causes a severy pneumonia in humans. The virus first appearance occurred in late Dec 2019 in China (Wuhan), after health officials noticed an increase in the incidence of pneumonia for no known cause in the city and gradually in other Chinese cities. Since then, the disease has spread throughout China and other parts of the world.Given the ability of the virus to transmit rapidly between individuals and the lack of specific treatment for the disease, it is critical to identify individuals in the early stages in order to quarantine them. According to WHO (the World Health Organization), as of June 16, 2021, there are 177,340,599 cases of infection and 3,836,166deaths.

Molecular testing has been introduced as a confirmatory test for this disease. Recently, there have been reports of false negative results in the initial molecular test of patients.Some of the reasons that can cause false negative results in the RT-PCR test include problems in sampling and transfer of samples, the efficiency of the kits used, and the quality of the test performed by the operator. Chest X-rays, on the other hand, are used as a routine imaging tool to diagnose lung pneumonia, which, given some common findings in the lungs of people infected with coronavirus, can yield rapid results.

In this non-invasive imaging technique, due to its high sensitivity in detecting coronavirus and its speed in producing high quality images of lung tissue, it can measure the involvement level of lung with coronavirus in a very short time[2,3]. Chest X-rays images of the lungs to diagnose coronary artery disease show pulmonary masses in the lungs, multifocal spots, and interstitial changes with peripheral distribution. Image processing and machine vision in recent years have been used severally as auxiliary methods along with the physicians to improve the diagnosis accuracy. Especially, in recent years, the deep learning application for the COVID-19 diagnosis has been exponentially increasing. Indeed, this technology can severlyanalyze and inform COVID-19 probability to the patients and physicians to provide a cost effective, fast quarantine and intensive care.

2. Context

Several research works are proposed for improving the COVID-19 diagnosis accuracy and indicate good outcomes in this subject.

In 2020, Wang et al [4] proposed a personalized CNN (Convolutional Neural Network) for the COVID-19 samples diagnosis using the pictures of the CXR(chest X-ray). Moreover, they presented a novel CXR open access benchmark COVID-19 database, namely COVIDx, that was gathered from 13,870 patient cases. Also, They explored about how their method provides predictions to achieve deeper insights associated with COVID cases for a proper diagnosis of this deseasefrom the CXR images.

In 2021, Khuzani et al. [5] employed a dimension reduction technique to provide optimal features from the CXR images to generate proper features for injecting ito the classifier and finally diagnosis of the COVID-19 samples from usual ones. A relatively small dataset of CXR imagesare used for training of the classifier. They proposed that the proposed method can be utilized in different test cases.

Motamed et al. [6] presented a RANDGAN (randomized generative antagonistic network) for the COVID-19 cases diagnosis and separate it from pneumonia and normal cases with no need for marks and training data. They used COVIDx dataset for the analysis. Transfer learning was used for segmentation of the lungs in the dataset. At last, the method was then compared with conventional generative adversarial networks to show the method effectiveness.

Maguolo et al. [7] investigated and compared different testing protocols utilized for the computer-aided COVID-19 diagnosis from the CXR images. They showed that using CXR images with least of the lungs provides similar results. They assumed that numerousrecognition testing protocols were not fair and also, neural networks were no longer related to the COVID-19 presence. At last, they showed that generating a fair testing protocol is difficult.

Narin et al. [8] analyzed five pre-trained CNNs to the diagnosis of the COVID pneumonia-infected cases in CXR images. 3 various binary categorizations with 4 classes, including COVID-19, normal, bacterial and viral pneumonia were cross-validated. The outcomes of simulation illustrated that the pre-trained ResNet50 model coud provide the largest ratio of accuracy for classification.

It can be observed that utilizing CXR imaging has better results for the COVID-19 disease diagnosis. Hence, in the present study,the method is performed on CXR images to deliver better diagnosis results. However, the results of the literature works are well, still lots of works can be implemented on the system to provide reliable and accurate results. In this sudy, we work on a new architecture of CNN to provide a proper system efficiency for the COVID-19 diagnosis from the CXR images.

3. Methodology

This section of this research presents the methodology employed in this research work to detect the disease from chest X-rays.

3.1 The study pipeline

In the suggested methodology, we have trained 19 layers convolutional neural network. The suggested model contains of four convolution layers. At the end, fully connected dense layers along with softmax and classification layer are considered with no repetition of convolution block. The suggested methodology pipeline diagram is represented in Fig. (1).

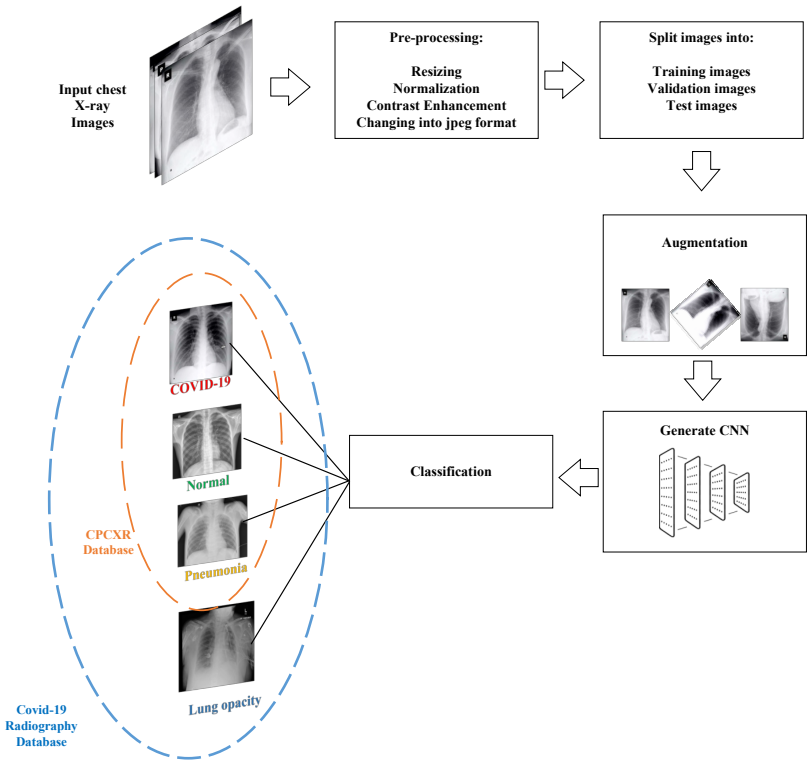

Fig. 1. The pipeline diagram of the offered methodology

Regarding Fig. (1), firstly, the original images of X-ray have been preprocessed. In this step, all of the images turned into the same size for analysis. Then, contrast enhancement and normalization of data are utilized for improving the images' quality. Then all of the images turned into the same format (.jpeg) to simplify the analysis. in the next step, the data divided into validation, training, and test data and all of the data are augmented. Then, the proposed CNN is designed based on the data and the final diagnosis has been done based on the proposed CNN.

3.2 Dataset Description

The present work uses images of CXR from 2 public datasetsincluding “Covid-19 Radiography Database” [9] and “Covid-19 Posteroanterior Chest X-Ray Fused (CPCXR) Dataset”[10]. The Radiography Database of Covid-19 is a CXR images data bank for positive samples of COVID-19, Viral Pneumonia, and Normal pictures that is created via investigators from the University of Dhaka, Qatar University, Bangladesh in the company of some researchers from Malaysia ad Pakistan and the medical doctors. This database includes 10,192 Normal, 1345 Viral Pneumonia pictures, 6012 Non-COVID infection of lung, and 3616 COVID-19 positive samples. This dataset can be achieved by downloading from https://ieee-dataport.org/documents/covid-19-posteroanterior-chest-x-ray-fused-cpcxr-dataset.

The second dataset is CPCXR (Covid-19 Posteroanterior CER Fused) which is created via the fusion of 3 accessible databases for public: RSNA (North America’s Radiological Society) (https://www.kaggle.com/c/rsna-pneumonia-detection-challenge), U.S. national library of medicine (USNLM) collected Montgomery country - NLM(MC) (https://lhncbc.nlm.nih.gov/publication/pub9931), and COVID-19 Chest X-Ray picture (https://github.com/ieee8023/covid-chestxray-dataset). These datasets are marked by expert physicians. The dataset includes examples of illnesses categorized as COVID-19 (1108), Other pneumonia (2515), Tuberculosis (358), and Normal (533). Fig. (2) shows some samples of COVID-19, Pneumonia, Normal, and lung opacity samples that are analysed in this paper.

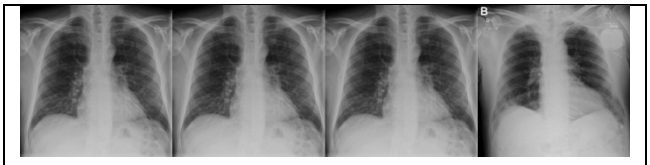

(A)

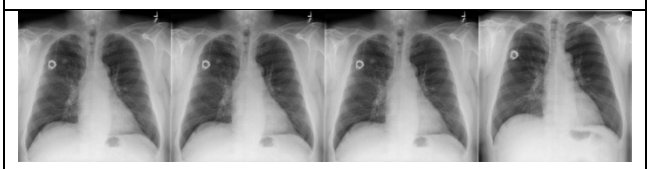

(B)

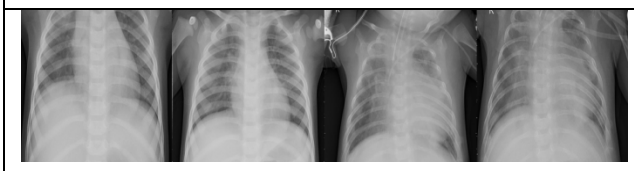

(C)

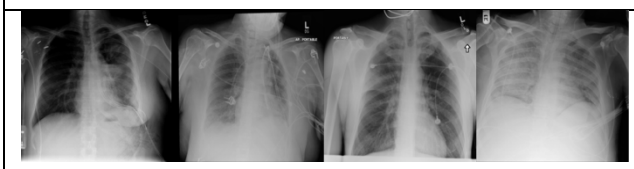

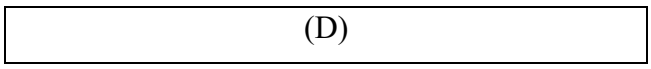

Fig. 2. Sample CXR images of (A) COVID-19, (B)Normal`, (C) Pneumonia, (D) Lung Opacity

Table 1 and Table 2 indicate more details about the utilized datasets.

Table 1. The details of the Covid-19 Radiography Database

Class	Dimension	Images		
		Total	Training	Validation
Normal	299×299×1	10,192	8,153	2,039
COVID19	299×299×1	3,616	2,892	724
Non-COVID lung infection	299×299×1	6012	4,809	1,203
Viral Pneumonia images	299×299×1	1345	1,076	269

Table 2. The details of the CPCXR Database

Class	Dimension	Images		
		Total	Training	Validation
Normal	224×224×1	533	426	107
COVID19	224×224×1	1108	886	222
Tuberculosis	224×224×1	358	286	72
Viral Pneumonia images	224×224×1	2,515	2,012	503

3.3 Dataset normalization

One scaling and mapping procedure in the preprocessing step of the data mining process is normalization. Thus, the data mapping from existing interval to anotherone is provided. This technique could be very helpful in analysis goals, so given the variety of images lightening models in medical imaging and in order

to maintain this variety, the methods of normalization assisst us to make an easier analysis for medical imaging[11]. This allows the data to be shorter in scope and the model to be better trained by the network.For clarification of the normalization, consider that the intervals of two characteristics (A and B) are completely different[3]. For instance, assume the interval for one characteristic is in the interval $[a_L, a_U]$ and the interval for the second characteristic is in the range $[b_L, b_U]$.Here if one characteristic, for example, A has a range smaller than the B, its effect on the evaluations[12]. Therefore, a pre-processing is needed to resolve this issue and change all of the intervals close to each other. Several normalization techniques have been introduced for solving this issue; the most prevalent onre, especially in image processing is Min-Max normalization. The Min-Max normalization method maps all of the intervals into an arbitrary interval where the minimum and the maximum can be predefined. In other words, any arbitrary interval can be selected to change all of the characteristics in it. Assume we want to map a charactyeristic, X, from its default interval in the range $X_L$andX_U to the new interval in the range X_L^{new} to X_U^{new}. This begins with an arbitrary initial value such as X in the initial range that is converted to the new value X^{new} as follows:

$$X^{new} = (X - X_L) \times \frac{X_U^{new} - X_L^{new}}{X_U - X_L} + (X_L^{new}) \quad (1)$$

3.4 Contrast enhancement

To extract detailed and clear information from the low-contrast regions in CXR pictures, we must enhance the images contrast. In the chest X-ray images enhancement, different methods like edge sharpening, filtering, and noise suppression has been considered [13]. In contrast enhancement, the range of brightness has been stretched in an image to advance the general or local contrast of the image to provide an image with higher details. In this study, Gamma correction has been used for contrast enhancement[14]f. Gamma correction is a suitable technique for removing the distortion from the Xray images. The Gamma correction is on the basis of histogram processing to enhance the image contrast quality using an adjustable parameter, Gamma (γ) [15].The Gamma correction is a nonlinear filter that modifies the image brilliance using the Gamma predefined factor. In an iput image, the TGC (transformed correction of gamma) has been mathematically achieved as follows:

$$TGC = I_M \left(\frac{I_i}{I_M}\right)^{\gamma} \quad (2)$$

where,I_i represents the image intensity, I_M signifies the maximum value for the input image intensity, and γdefines an adjustable factor in the the range [0,∞).

The Gamma factor, in the above formula, varies the image's pixel intensity. When Gamma is equal to one, no changes will exist on the original picture. Conversely, when $\gamma < 1$, the brilliance of the picture is increased and if $\gamma > 1$, the vividness of the image is decreased[16]. This shows the importance of correct

selection of the Gamma value. several works have been proposed for this purpose. Here, we used the method of [17].Fig. (3) shows some contrast enhancement examples for the CXR images.

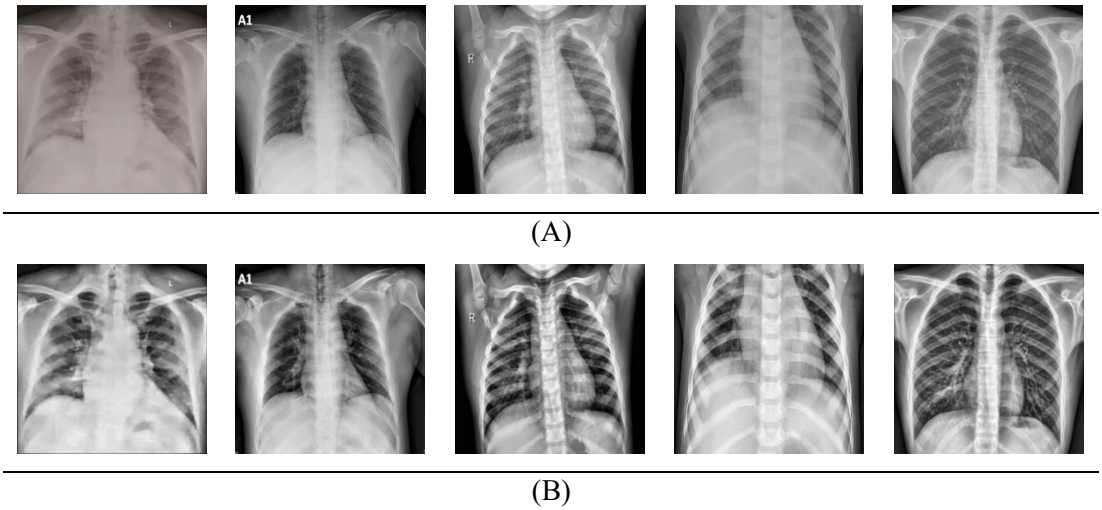

(A)

(B)

Fig. 3. Some contrast enhancement examples for the CXR images.

3.5 The Proposed Network Design

This section discusses about the proposed 19-layer CNN model for the COVID-19 diagnosis from the CXR pictures. The suggested network containfive main components including convolutional layer, pooling layer, batch ormalization, fully connected layer, and function of activation that have been employed in diverse layers of the network. In the following, the detailedexplanations about these layers have been discussed.

3.5.1 *Convolutional* layer

The CNN convolution process happens and the model is trained in this layer. The convolution layer is the core of the convolution NN, the production mass of this layer can be interpreted as a three-dimensional mass of neurons. In the CNN model, a big share of the evaluations is performed. These layers extract features on the basis of the filters and afterwards uses them for training. In this layer, some features are extracted from the original pictures, and subsequantly, on the basis of the image matrix, a dot product is generated for providing some matrices. The filter's size has been the most crucial factor in convolution neurons. In the offered technique for COVID-19 cancer classification, 4 layers with different sizes of filters, including 64 channels($3 \times 3 \times 32$), 32 channels ($3 \times 3 \times 16$), 16 channels ($3 \times 3 \times 8$), and 8 channel ($3 \times 3 \times 1$) are utilized. Feature maps have been made by multiplying these filters matrices by the images. For generating the feature map, the filter moves from up to down and left to right with a specific stride

dimension to extract high-level characteristics (like edges) as far as it does finish the whole width[18]. The convolutional layer output is achieved using the following equation:

$$y_j^i = f\left(\sum_{a=1}^{M} w_j^{l-1} * x_a^{l-1} + b_j^l\right) \quad (3)$$

where, x_a^{l-1} defines the a^{th} feature map in layer $l-1$,w_j^{l-1} signifies the j^{th} kernels in layer $l-1$, y_j^i describes the j^{th} feature map in layer l, M describes the number of total features in layer $l-1$,b_j^lrepresents the bias for the j^{th} feature map in layer l, and $(*)$ describes the convolution process vector.

3.5.2 *Pooling* layer

This layer reduces the spatial size in width and height (not depth). Accordingly, this process is used to subsample the input image and decrease the number of parameters, and concequently decreases the valume of the calculations and increases the network speed. The represented work utilizes 2 × 2 Maximum Pooling with [0 0 0 0] padding and [2 2] pace. The process of Max-pooling utilizes the feature maps' highest amount to shrink the produced neurons. Mean pooling layer is also utilized prior to the FC (Fully-Connected) layer to reduce the data to one dimension.

3.5.3 *Fully* Connected (FC) layer

Three channel fully connected layer has been utilized after the pooling and convolution layers. FC layer determines the features which mostly match to a specific class. It works on high-level features with specific weightiness. Indeed, this layer affords the exact probabilities for the diverse classes by producting the weights with the earlier layer. The outcomes are categorized using the function of activation.

3.5.4 *Activation* function

A layer of activation is utilized after every convolution layer; it is used for introducing non-linear operations to a linear operation system along the computation layers. In the represented study, the activation function is *Sigmoid function*. This function is formulated below:

$$f(x) = \frac{1}{1 + \exp(-x)} \quad (4)$$

where the sigmoid function is a S-shaped curve between 0 and 1.

This is done with Rectified linear unit (ReLU) function .The RELU layer does apply $f(x)$ to whole original pictures and changes whole negative activities to nil. Having utilized this layer, the model and network nonlinear properties are enhanced without affecting the concentration layers. The formulation of this layer is as follows:

$$RELU = \max(0, x) \tag{5}$$

where, x is a real value.

We also use Softmax activation function in the last layer to normalize the network output in interval of (0,1). The equation for the Softmax activation function is given below:

$$Softmax(x_i) = \frac{\exp(x_i)}{\sum_{j=1}^{N} \exp(x_j)} \tag{6}$$

where, x_i and N represent the original data and the classes number. Fig. (4) and Fig. (5) shows the convolution#1, convolution#2, convolution#4, and Fully connected layers to have a comprehensive conception from the metwork.

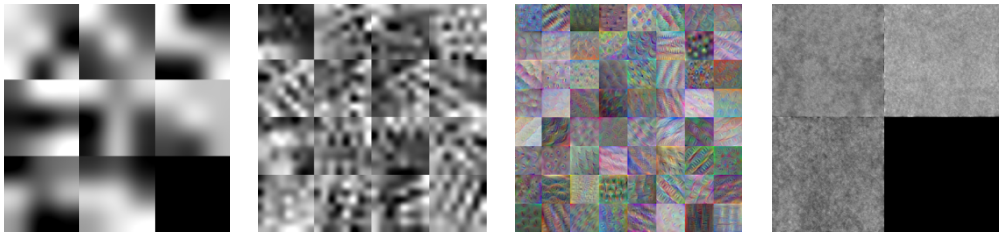

(A) (B) (C) (D)

Fig. 4. The (A) convolution#1, (B) convolution#2, (C) convolution#4, and (D) Fully connected layers for CPCXR dataset

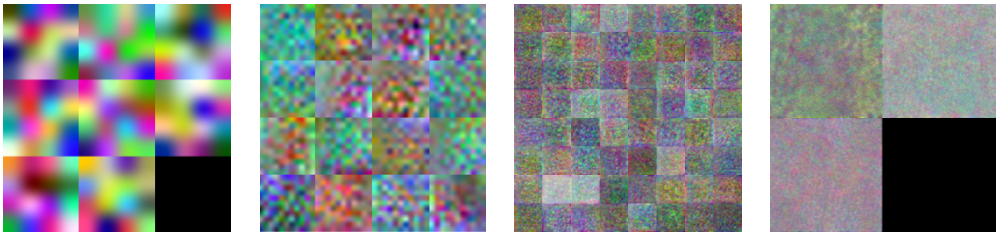

(A) (B) (C) (D)

Fig. 5. The (A) convolution#1, (B) convolution#2, (C) convolution#4, and (D) Fully connected layers for Covid-19 Radiography database

The detailed design of the proposed CNN Model is represented in Table 3.

Table 3. The Structur of the designed CNN

Layer	Params	Activation	Output
Input	-	-	227×227×1
Convolution #1	Stride(St) [1 1], Padding(Pd) 'Same'	ReLu	8@3×3×1

Batch Normalization #1	-	-	8 channels
MaxPooling#1	St [2 2], Pd [0 0 0 0]	-	2×2
Convolution #2	St [1 1], Pd 'Same'	ReLu	16@3×3×8
Batch Normalization #2	-	-	16 channels
MaxPooling#2	St [2 2], Pd [0 0 0 0]	-	2×2
Convolution #3	St [1 1], Pd 'Same'	ReLu	32@3×3×16
Batch Normalization #3	-	-	32 channels
MaxPooling#3	St [2 2], Pd [0 0 0 0]	-	2×2
Convolution #4	St [1 1], Pd 'Same'	ReLu	64@3×3×32
Fully connected	-	Softmax	3 layers
Output Classification	Crossentropyex	-	3 outputs

3.6 Pre-trained Models

To provide a proper analysis of the proposed method, we used some *Transfer Learning*-based pretrained networks. Transfer learning (TL) has been a ML (machine learning) technique where, a model development is implemented for a task that is restated as the model beginning point in another task. TL is by far the most common method of DL (deep learning). For example, in this method, pre-trained models have been utilized as a beginning point in computer image. TL is employed for extending pictures out of the ImageNet database. This only does happen with a pre-trained (pt) model. Thus, we employ a model of fine tuning derived from the modification of a pt model. We do not aim to change the weights too much and soon on the grounds that we consider that the network is already well trained. When changing occurs, we usually utilize a rate of learning that is lower compared to that used in the basic model tutorial. In the presented research, deep CNN-based Alexnet, GoogLeNet (Inception), ResNet50, Squeezenet, VGG19 models are utilized for the COVID-19 diagnosis in CXR images for 2different datasets with three and four different classes. All of the pretrained networks are realized by employing the Deep Learning Toolbox to weather the inadequate time of training and data.

3.6.1 Alexnet

AlexNet has been considered the 1st deep architecture to be presented by Hinton, Geoffrey and et.al. AlexNet architecture is straightforward but powerful that paved the way for great investigation without which there would be no in-depth learning of what it is now.

When we open AlexNet, its architecture seems straightforward with complex layers placed on top of other layers and entirely linked to the layers situated on top. This is a very simple architecture, the concept of which first appeared in the 80s. Thje main character of this model which does make it different is the task velocity and the use of a "GPU" for learning.

3.6.2 GoogLeNet

In GoogLeNet, a module named Inception, was designed via the attitude of developing the parameters of network hyper into the learnable factor. A pooling filter and 3 CFs (convolutional filters) with diverse dimentions are employed on the prior layer in Inception, then the outcomes are put together as a tensor. In this case, the network can decide in the next layer which filter it wants to use and to what extent. The size of convolutional filters is 1×1, 3×3, and 5×5 and the polishing filter with 3×3 size is applied on it.In this network, by placing two layers of polishing at the beginning of the work, the learnable parameters of the problem are greatly reduced. In the following, 9 layers of Inception module are used. More details can be achiebed by [19].

*3.6.3 ResNet50 (*Residual Network*)*

This network was provided by Microsoft. In ResNet50, communication out of the convolutional arrangement has been provided next to the network between layers to transfer the inputs of the former layer to the following one without mediators. Every layer's error in the back propagation step is transferred to the former layer; accordingly, the network becomes capable of faster training and deepening. Such associates have been addressed *skip connections*. Moreovere, the resulting arrangement is addressed *Residual block*. With such trick, they were able to train a 152-layer network.

3.6.4 Squeezenet

SqueezeNet architecture is a very powerful architecture that is very efficient in places with little space, including cell phones. This architecture only takes up about 5MB of space, while the "inception" model takes up about 100MB. This big change is possible thanks to a special architecture called the fire module.

3.6.5 VGG19

When it comes to complexity, this network is simpler compared to AlexNet on the grounds that it lessens the HyperParameters' quantity; for that reason it is very common and desirable. In VGG CONV is 3 × 3 filter with 3 and same stride and POOL means 2 × 2 pulling, with stride 2.

4. Results and Discussions

4.1 Network Architecture and system configuration

Table 1 and Fig. (6) illustrate an instantaneous description of our suggested 19-layer Convolutional Neural Network. From Table 1 and Fig. (6), it is observed that the suggested 19-layer CNN model owns four Conv2d and three max-pooling2d layers. In the layers 3, 7, 11, and 15, Batch normalization is utilized with 8, 16, and 32 channels for enhancing the stability of the model by employing standardization on the input size. stochastic gradient descent with momentum (SGDM) optimizer has been used for updating the function of cross-entropy loss, weight updates, and chosen learning ratio. Maximum iteration is considered 440 and 2.6e4 with almost 6 epochs for Covid-19 Radiography and CPCXR datasets, respectively, and the initial learning rate is set 0.0001.

The main purpose in designing the suggested CNN model is to deliver the finest arrangement with the maximum accuracy for the model by considering activation functions, the layers, and optimizer values. The model is designed over a rigorous testing process with testifying different numbers of layers, altering the optimizers' value, and changing activation functions, For instance, the task commences with a simple 9-layer CNN model, that provided 74 % accuracy for the Covid-19 Radiography Database and 80 % for the CPCXR datase. The ReLu is selected as the best model for activation function. Then, we used more layers to provide better reults by considering an agreement among accuracy and the time complication. Table 4 reports the configuration of the system that simulations are carried out.

Table 4. The system configuration employed in this study.

Name	Setting
Hardware	Intel® Core™ i7-4720HQ
CPU	1.60 GHz
RAM	16 GB
Frequency	1.99 GHz
Operating system	Windows 10
Programming software	MATLAB R2019b

The time complexity for learning the network for CPCXR and Covid-19 Radiography databases is 172.8919 seconds and 7672.464356 seconds, respectively. After selecting the best activation function, the number of Conv2D as a convolutional layer are selected. This is done based on providing a good balancing between accuracy and the time complexity based on our system configurstion. The outcomes demonstrated that the offered model has finer outcomes compared to the pretrained models for our purpose. Training network is established based on two independent datasets with 3 (for CPCXR) and 4 classes (for the Covid-19 Radiography data) by considering the labeled data to identify chest X-ray images. The simulations are

implemented using Deep Learning Toolbox. Fig. (6) depicts the descriptive block plan of the offered CNN architecture

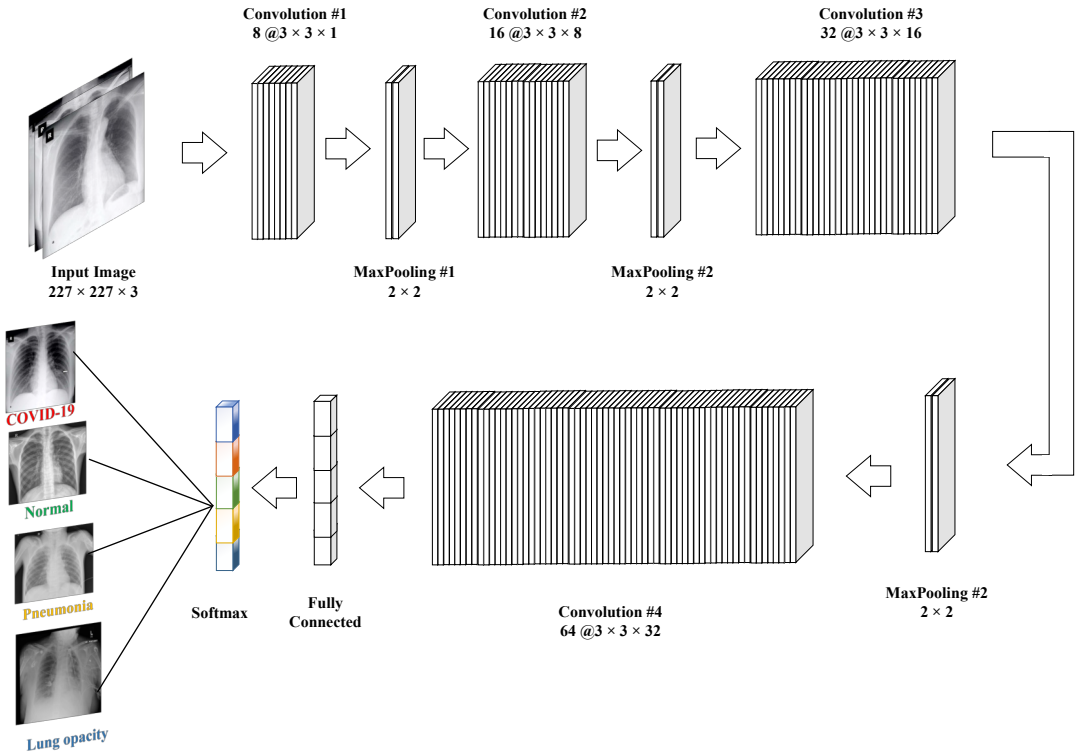

Fig. 6. Descriptive block diagram of the proposed CNN architecture

Random initialization weights is used to pre-train of the studied transfer learning-based CNN models (Alexnet, GoogLeNet (Inception), ResNet50, Squeezenet, VGG19) by optimization of the function of cross-entropy via ADAM (adaptive moment estimate) optimization approach ($\beta_1 = \frac{9}{10}$and $\frac{999}{1000}$). The learning rate, size of batch, and repetition number were considered 10^{-5}, 3, and 30 based on experiments. The datasets have been randomly splitted into 2 seprate databases with twenty percent for testing and eighty percent for training.

4.2 Performance metrics

In this study, five measurement indicators are utilized for assessing the performance of the suggested system. The mathematical formulation of the measurement indicators are given below:

$$Accuray = \frac{TP + TN}{TP + TN + FP + FN} \tag{7}$$

$$Specificity = \frac{TN}{TN + FP} \tag{8}$$

$$Sensitivity = \frac{TP}{TP + FN} \tag{9}$$

$$Precision = \frac{TP}{TP + FP} \tag{10}$$

$$F1 - score = \frac{2 \times Precision \times sensitivity}{Precision + sensitivity} \tag{11}$$

where, TP, TN, FP, and FN represent True Positive that predicts a positive case correctly, True Negativepredicts a negative case correctly, False Positive predicts positive case mistakenly, and False Negativepredicts negative case mistakenly, respectively. Fig. (7) shows this conception.

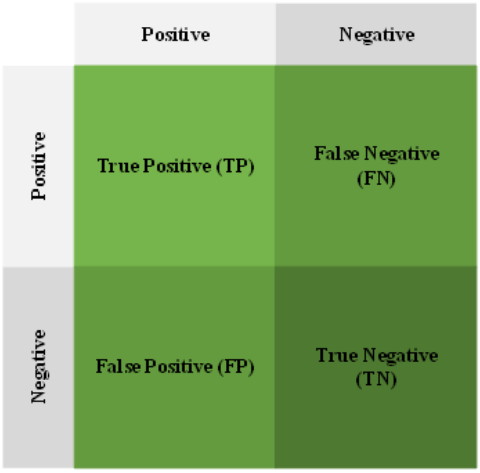

Fig. 7. The conception of the measurement indiators

In Eq. (7)-Eq. (11), accuracy measures the classifier accuracy to isulate between normal, COVID-19, bacterial and viral pneumonia samples. Precision determines the related cases fraction among the recovered cases that are recognized as the positive predicting amount. Sensitivity assesses the correctly classified ratio of the positive instances. Specificity defines the portion of the correctly classified negative instances, and F1-score explains the test accuracy being definite as the precision weighted harmonic mean.

4.2.1 Evaluations

To provide a proper analysis for the suggested CNN model, different measurement indicators, including accuracy, sensitivity, specificity, F1-score, precision, and confusion matrix for all datasets have been assessed. The descriptionsfor accuracy, specificity, sensitivity, precision, and F1-score can be achieved in[20]. Tables 5 reports the offered CNN performance in comparison to some published methods including Alexnet[21], GoogleNet(Inception)[22], ResNet50 [23], Squeezenet[24], and VGG19 [25] considering the metrics precision, accuracy, specificity, F1-score, and sensitivity.

Table 5. The comparison results between the proposed CNN and other studied networks for COVID-19 diagnosis.

Datasets	Procedure	Performance Metric				
		Accuracy	Specificity	Precision	Sensitivity	F1-score
CPCXR	Inception[22]	89.17	89.13	90.53	91.57	90.36
	Alexnet[21]	87.43	83.19	74.66	86.19	79.54
	ResNet50 [23]	82.90	62.28	66.05	84.73	74.93
	Squeezenet[24]	67.28	57.26	58.34	82.94	68.22
	VGG19 [25]	83.69	79.57	76.11	81.09	78.46
	Proposed CNN	98.40	91.13	89.54	91.30	87.09
Covid-19 Radiography	Inception[22]	87.49	86.95	88.37	89.01	88.26
	Alexnet[21]	85.36	81.24	72.16	84.67	77.18
	ResNet50 [23]	80.29	60.73	64.51	81.16	72.08
	Squeezenet[24]	65.24	55.18	56.76	80.35	66.27
	VGG19 [25]	81.33	77.64	74.10	79.36	75.42
	Proposed CNN	97.51	89.60	87.59	88.43	86.91

With regard to Table 5, the studied CNN offers superior results in terms of accuracy. Accordingly, This network is a good selection for the consistently diagnosis of the COVID-19 from the other cases.

Regarding Table 5, the offered CNN with 98.40 % and 97.51 % accuracy, supplies the maximum efficiency. Similarly, Inception method with 89.17 % and 87.49 % for CPCXR and Covid-19 Radiography, respectivelyhas the 2nd ststus in the comparison. Also, Alexnet, VGG19, ResNet50, and Squeezenet methods are ranked in the next places. Also, the suggested method with 91.30 % and 88.43 % sensitivity for CPCXR and Covid-19 Radiography, respectively as the max amount against the others, specifies the more consistency of the procedure compared to other methods. Also, higher Precision of the offered technique intitles its higher circumstance happening for controling a test likelihood in disease identification. What is more, higher Specificity value of the proposed mthod indicates its advanced happening-independent attainment.

Based on the optimized trained CNN, however the first training time for CPCXR and Covid-19 Radiography datasets are 165.8434 seconds and 13389 seconds, respectively, the testing step of the images for both data are less than 10 s. Fig. (8) shows the ROC (Receiver Operating Characteristic) profile of the proposed CNN compared with other studied networks.

Therefore, the results from Table 3 indicate satisfying results for the proposed model. In Fig. (8), the analysis of the confusion matrix for the proposed CNN architecture implemented on CPCXR and Radiography datasets is shown.

CPCXR dataset | Radiography dataset

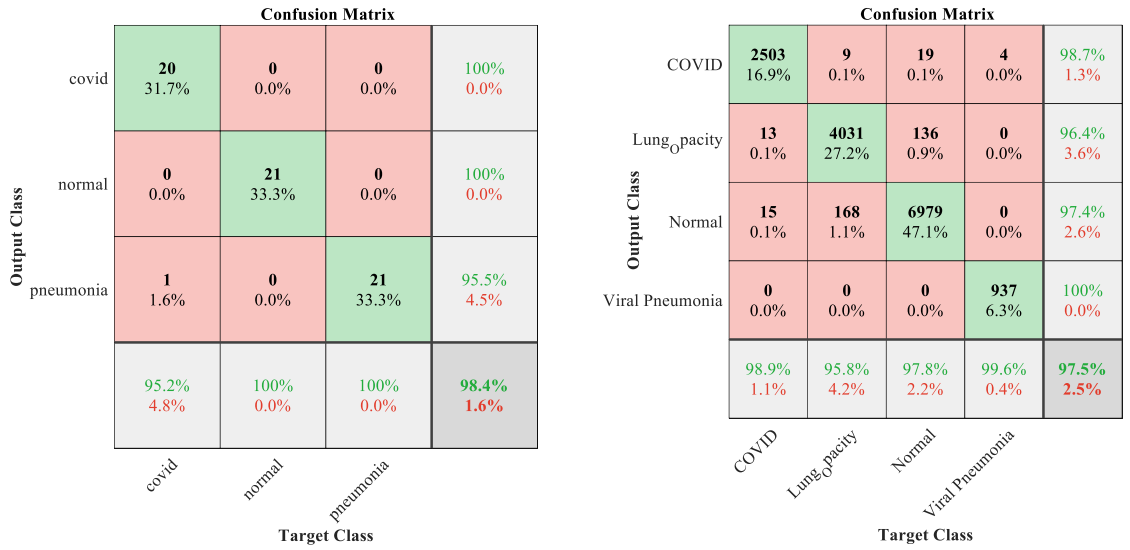

Training

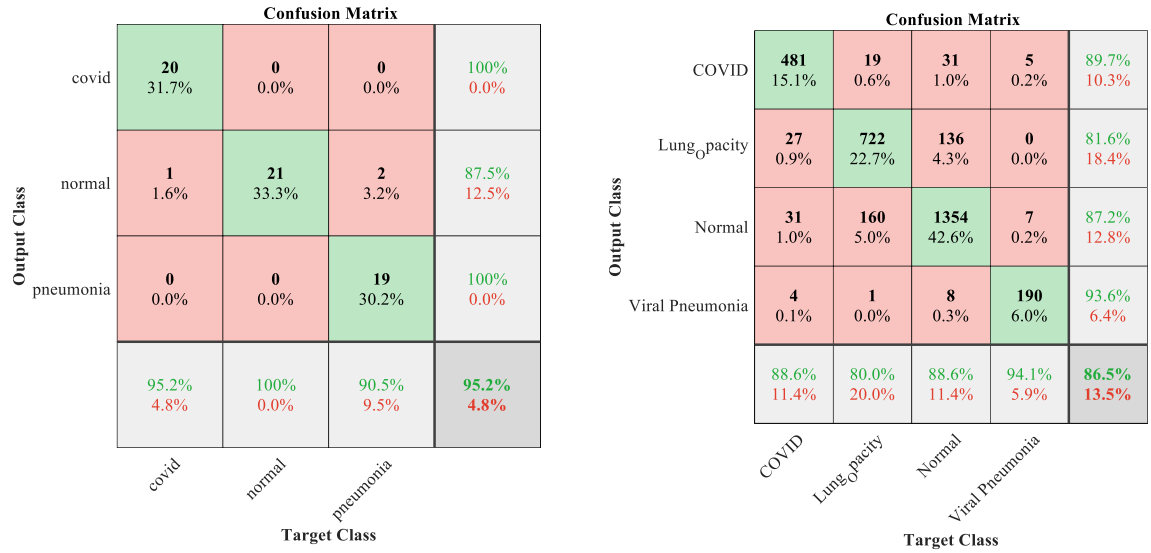

Validation

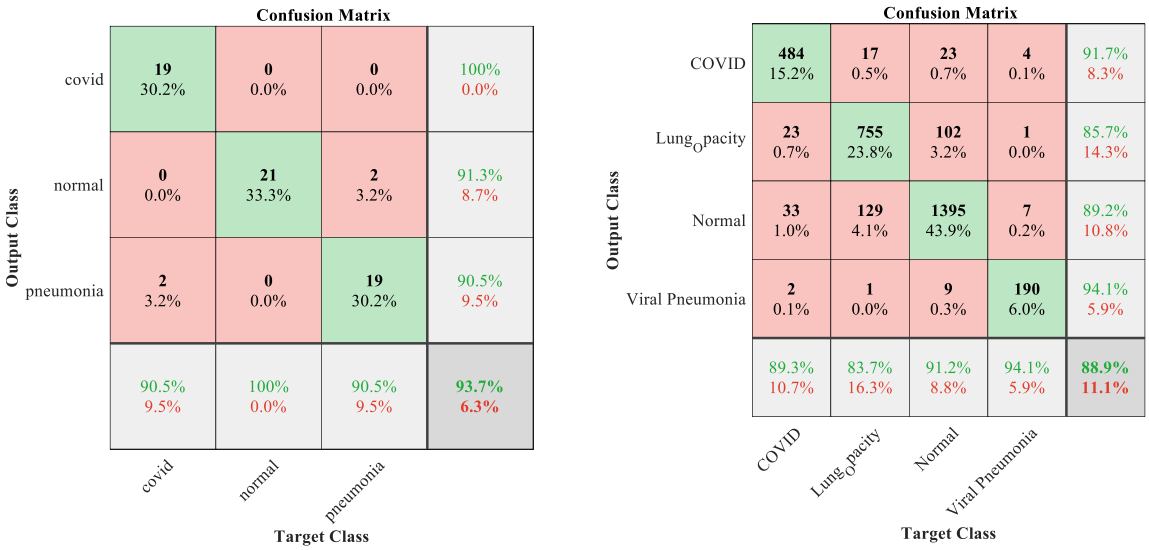

Test

Fig. 8. The evaluation of Confusion matrix of the offered CNN architecture implemented on CPCXR and Radiography datasets

As can be observed, For both three-fold and four-fold classifications, the proposed model provides a satisfying efficiency for both datasets.

The accuracy and loss of the model for the CPCXR and the Covid-19 Radiography Database datasets are depicted in Figs. (9)and (10).

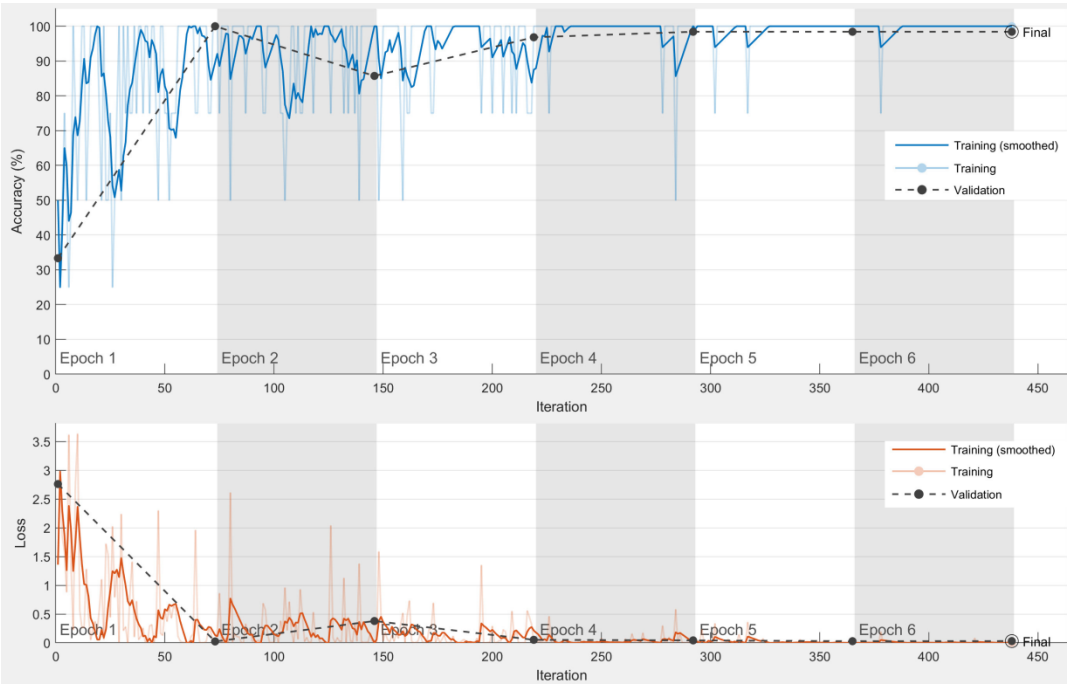

Fig. 9. Training progress of the offered CNN on the basis of accuracy and loss for CPCXR dataset

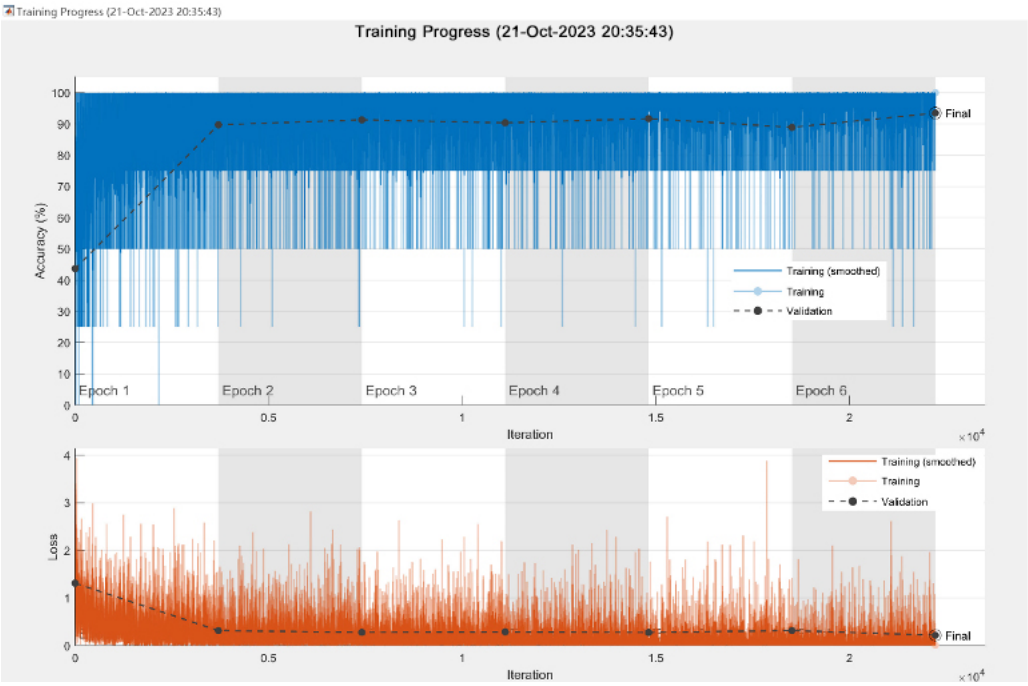

Fig. 10. Training progress of the proposed CNN based on accuracy and loss for Covid-19 Radiography Database dataset

As can be observed from Fig. (9) and Fig. (10), the offered CNN model with 19 layers has been trained excellently with no underfitting and overfitting. The figures clarify that why better results are achieved when it comes to Accuracy, Specificity, Precision, confusion matrix, F1-score, and Sensitivity. The plots demonstrate the accurately training process of the model. The ROC curve for two studied datasets and for the proposed 19-layer CNN model compared with the best model from Table 3 (Inception model) are shown in Fig. (11). The ROC plot is the TPR versus FPR (True Positive versus False Positive Rates). This signifies the model diagnostic capabilitywith analysingthe separability degree among different classes. Based on ROC figure, higher AUC (Area Under the Curve) depicts the method efficiency, such that if AUC is 1.0, the model is in its best condition and if it is 0, it provides a poor model.

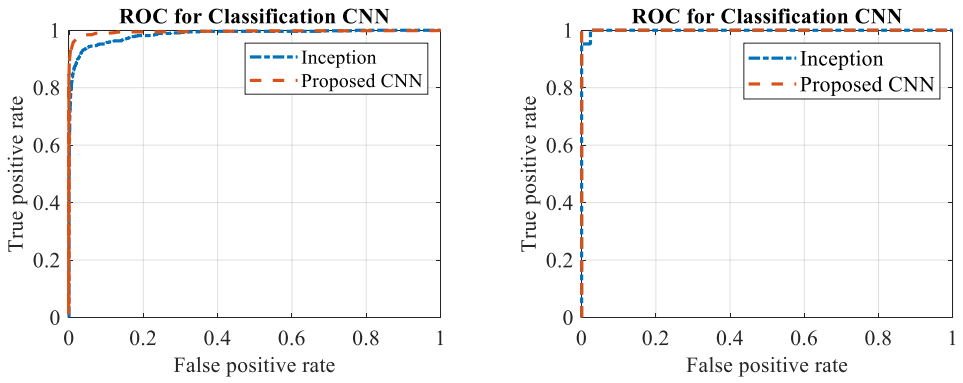

(A) (B)

Fig. 11. The ROC profile for the proposed CNN compared with Iceptionfor (A) Covid-19 Radiography Database dataset and (B) CPCXR dataset

Regarding Fig. (11), the average AUC for the proposed method for Covid-19 Radiography Database dataset and CPCXR datasetis 1.0 and 0.99, respectively while in both , the proposed model has higher AUC compared to the inception one. Finally, Fig. (12) and Fig. (13) show some classification examples of the offered procedure on CPCXR and Covid-19 Radiography Database datasets.

4.2.2 Discussions

Because of the rapid and global growth of theCOVID-19, there is a need tofast and accurately diagnosis of this disease. In the present study, a new 19-layer CNN model is proposed to separate COVID-19 patients from Viral Pneumonia, Lung Opacity, and Normal in CXR pictures in two different datasets.

Due to proper and efficient results of the CXR images, they are utilized in most hospitals. The proposed CNN network was trained, validated and tested by 21165 images from Covid-19 Radiography Database and by 4514 images fromCPCXR dataset. 70% of the data are used in training process and 30% of them are employed for validation and test. The method provides 93.7 % and 88.9 % accuracyforCovid-19 Radiography Database and CPCXR dataset, respectively which is the best result in comparison with the other assessed techniques in the study. Comparison outcomes show the prominence of the suggested CNN toward the other pretrained networks. Therefore, this can be considered as a useful tool for the doctors and clinitiansto provide more precise results. As can be concluded, The proposed method has also some shortcomings. One limitationsis that the proposed CNN does not encode the orientation position of the input images which makes us to provide some preprocessing steps. Also, the proposed CNN has some numbers of adjustable parameters that should be carefully selected especially we have a great deal of parameters.

Figs. (12) and (13) depict the outcomes of the offered model for CPCXR dataset and Covid-19 Radiography Database dataset, respectively.

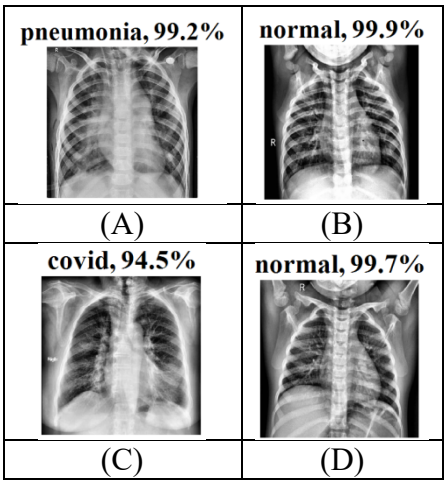

Fig. 12. Some classification samples of the proposed method on CPCXR dataset

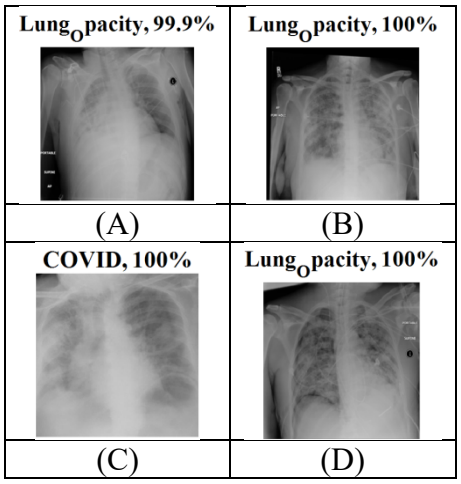

Fig. 13. Some classification samples of the proposed method on Covid-19 Radiography Database dataset

5. Conclusions

In late 2019, many worries exsited about the spread of a new respiratory ailment (Covid-19) and ways to cope with it. Given the virus fast spread, it is crucial to identify infected individuals in the early stages for quarantine. The COVID-19 is a pandemic ailment began by infection with a virus which recently causes many deathsin different countries. Timely and quick identification of this disease is a significant subject not only to avoid from the outbreak of it, but also, to decrease the risk of the death. These days, a number of techniques are utilized to diagnose the COVID-19 disease, like sickness-correlated signs, and more precise diagnostic approaches, such as X-ray pictures of chest. In this work, the aim was to attain a precise diagnostic technique for automatic and intelligent identification of COVID-19 via CXR (chest X-ray) pictures and image processing methods as an accurate diagnostic tool as an X-ray supplement from public

references. This research introduced a different 19-layer CNN structure for the COVID-19 identification from the CXR images. Here, pre-processing of images was utilized on the input pictures. Pre-processing steps were resizing, normalization, contrast enhancement, and unifirm all images formats to a defined format. Then, the achieved images were splitted into training and test images randomly. Then, a data augmentation was performed to the images to increase the number of sample sets. Afterwards, the proposed 19-layer CNN was performed to the datasets an the final results were achieved. Simulations were performed to 2 public datasets including "Covid-19 Radiography Database" and "Covid-19 Posteroanterior Chest X-Ray Fused (CPCXR) Dataset". By comparing the proposed CNN with some popular pretrained networkswith employing Specificity, Accuracy, Sensitivity, F1-score, and Precision the offered model indicated the finest efficiency toward them.

Data Availability

The dataset can be downloaded from:

The first dataset: https://ieee-dataport.org/documents/covid-19-posteroanterior-chest-x-ray-fused-cpcxr-dataset.

The second dataset: https://www.kaggle.com/tawsifurrahman/covid19-radiography-database?select=COVID-19_Radiography_Dataset

References

[1] Ranjbarzadeh, R. *et al.* Lung infection segmentation for COVID-19 Pneumonia based on a cascade convolutional network from CT images. *BioMed Research International***2021** (2021).

[2] Ranjbarzadeh, R. & Saadi, S. B. Automated liver and tumor segmentation based on concave and convex points using fuzzy c-means and mean shift clustering. *Measurement***150**, 107086 (2020).

[3] Ranjbarzadeh, R. *et al.* Brain tumor segmentation based on deep learning and an attention mechanism using MRI multi-modalities brain images. *Scientific Reports***11**, 1-17 (2021).

[4] Wang, L., Lin, Z. Q. & Wong, A. Covid-net: A tailored deep convolutional neural network design for detection of covid-19 cases from chest x-ray images. *Scientific Reports***10**, 1-12 (2020).

[5] Khuzani, A. Z., Heidari, M. & Shariati, S. A. COVID-Classifier: An automated machine learning model to assist in the diagnosis of COVID-19 infection in chest x-ray images. *Scientific Reports***11**, 1-6 (2021).

[6] Motamed, S., Rogalla, P. & Khalvati, F. RANDGAN: randomized generative adversarial network for detection of COVID-19 in chest X-ray. *Scientific Reports***11**, 1-10 (2021).

[7] Maguolo, G. & Nanni, L. A critic evaluation of methods for covid-19 automatic detection from x-ray images. *Information Fusion***76**, 1-7 (2021).

[8] Narin, A., Kaya, C. & Pamuk, Z. Automatic detection of coronavirus disease (covid-19) using x-ray images and deep convolutional neural networks. *Pattern Analysis and Applications*, 1-14 (2021).

[9] T. Rahman, M. C., A. Khandakar. *COVID-19 Radiography Database - COVID-19 Chest X-ray Database*, <https://www.kaggle.com/tawsifurrahman/covid19-radiography-database?select=COVID-19_Radiography_Dataset> (2020).

[10] Narinder Singh Punn, S. A. *COVID-19 Posteroanterior Chest X-Ray fused (CPCXR) dataset*, <https://ieee-dataport.org/documents/covid-19-posteroanterior-chest-x-ray-fused-cpcxr-dataset> (

[11] Razmjooy, N. *et al.* Computer-Aided Diagnosis of Skin Cancer: A Review. *Current Medical Imaging* (2020).
[12] Xu, Z., Sheykhahmad, F. R., Ghadimi, N. & Razmjooy, N. Computer-aided diagnosis of skin cancer based on soft computing techniques. *Open Medicine***15**, 860-871 (2020).
[13] Qin, C., Yao, D., Shi, Y. & Song, Z. Computer-aided detection in chest radiography based on artificial intelligence: a survey. *Biomedical engineering online***17**, 1-23 (2018).
[14] Razmjooy, N., Ramezani, M. & Ghadimi, N. Imperialist competitive algorithm-based optimization of neuro-fuzzy system parameters for automatic red-eye removal. *International Journal of Fuzzy Systems***19**, 1144-1156 (2017).
[15] Huang, S.-C., Cheng, F.-C. & Chiu, Y.-S. Efficient contrast enhancement using adaptive gamma correction with weighting distribution. *IEEE transactions on image processing***22**, 1032-1041 (2013).
[16] Niblack, W. *An introduction to digital image processing*. Vol. 34 (Prentice-Hall Englewood Cliffs, 1986).
[17] Agarwal, M., Rani, G. & Dhaka, V. S. Optimized contrast enhancement for tumor detection. *International Journal of Imaging Systems and Technology***30**, 687-703 (2020).
[18] Hussain, E. *et al.* CoroDet: A deep learning based classification for COVID-19 detection using chest X-ray images. *Chaos, Solitons & Fractals***142**, 110495 (2021).
[19] Yao, X., Wang, X., Karaca, Y., Xie, J. & Wang, S. Glomerulus Classification via an Improved GoogLeNet. *Access***8**, 176916-176923 (2020).
[20] Zhao, Y. *et al.* Early detection of ST-segment elevated myocardial infarction by artificial intelligence with 12-lead electrocardiogram. *International journal of cardiology***317**, 223-230 (2020).
[21] Cortés, E. & Sánchez, S. Deep Learning Transfer with AlexNet for chest X-ray COVID-19 recognition. *IEEE Latin America Transactions***19**, 944-951 (2021).
[22] Yu, X., Wang, S.-H., Zhang, X. & Zhang, Y.-D. in *International Conference on Intelligent Computing.* 499-509 (Springer).
[23] Walvekar, S. & Shinde, D. Detection of COVID-19 from CT images using resnet50. *Detection of COVID-19 from CT images using resnet50 (May 30, 2020)* (2020).
[24] Ucar, F. & Korkmaz, D. COVIDiagnosis-Net: Deep Bayes-SqueezeNet based diagnosis of the coronavirus disease 2019 (COVID-19) from X-ray images. *Medical hypotheses***140**, 109761 (2020).
[25] Das, A. K., Kalam, S., Kumar, C. & Sinha, D. TLCoV-An automated Covid-19 screening model using Transfer Learning from chest X-ray images. *Chaos, Solitons & Fractals***144**, 110713 (2021).